

**STABLE MAGNESIUM ISOTOPE VARIATION IN MELILITE MANTLE OF ALLENDE TYPE B1 CAI EK 459-5-1.** A. G. Kerekgartyo<sup>1</sup>, C. R. Jeffcoat<sup>1</sup>, T. J. Lapen<sup>1</sup>, R. Andreasen<sup>1</sup>, M. Righter<sup>1</sup>, D. K. Ross<sup>2</sup>  
<sup>1</sup>Department of Earth and Atmospheric Sciences, University of Houston, Houston Tx 77204 (agkerekartyo@uh.edu), <sup>2</sup>Jacobs, NASA-JSC, Houston Tx 77058

**Introduction:** Ca-Al-rich inclusions (CAIs) are the earliest formed crystalline material in our solar system [1] and they record early Solar System processes. Here we present petrographic and  $\delta^{25}\text{Mg}$  data of melilite mantles in a Type B1 CAI that records early solar nebular processes.

**Petrography and Major Element Chemistry:** EK 459-5-1 is a type B1 CAI measuring roughly 13.5 by 7.5mm, on loan from the Houston Museum of Natural Science. It is characterized by a spinel-fassaite-anorthite-melilite bearing core, with a ~2mm mantle of zoned melilite, indicative of the B1 classification [2]. Minor occurrence of 1-5  $\mu\text{m}$  grains of fassaite and spinel in the melilite mantle. Distinct spinel-free islands (SFI) within the core (Fig. 1a) are Na-enriched, as observed in [3]. Interior fassaite shows subtle sector zoning as well as a sharp ‘chaotic’ [4] zoning. The melilite mantle occurs in solid solution between gehlenite ( $\text{Ca}_2\text{Al}_2\text{SiO}_7$ ) and åkermanite ( $\text{Ca}_2\text{MgSi}_2\text{O}_7$ ). The mantle has two concentric textural types. An outer section is texturally massive and chemically zoned and an inner section that contains 3 or 4 bands of Mg, Al and Si oscillatory chemical zoning in the melilite (Fig. 1c). These bands typically contain small fassaite grains in alignment with the bands. Between the mantle and core, there is a sharp change in melilite composition and the occurrence of additional phases (Fig. 1c). Along the core boundary and borders of SFIs, spinel exists in linear agglomerations of an almost ‘wall-like’ texture. Preliminary  $^{26}\text{Al}$ - $^{26}\text{Mg}$  data indicates that this CAI formed while  $^{26}\text{Al}$  was extant.

**Methodology:** Initial petrographic work was done at JSC through ARES laboratories. X-ray elemental maps were produced on a JEOL JSM-7600F SEM and major element data was collected with a Cameca SX-100 electron microprobe. *In-Situ* isotope studies have been done on a Nu Plasma II MC-ICP-MS and Analyte 193nm excimer laser system. The laser was operated with a spot size of 50  $\mu\text{m}$ , 10 Hz rep rate, and a fluence of 2.99  $\text{J}/\text{cm}^2$ . Natural gehlenite standards were used to correct for instrumental isotope fractionation. Data is reported in  $\delta$  notation relative to DSM3 [5].

**Results:** Both line scans show a positive enrichment in  $\delta^{25}\text{Mg}$ , expected from early evaporative processes [6], and a sharp rim ward decrease in  $\delta^{25}\text{Mg}$  (Fig. 2). No definitive correlation can be made between  $\text{Åk}_\#$  and  $\delta^{25}\text{Mg}$ . Both vary as a function of

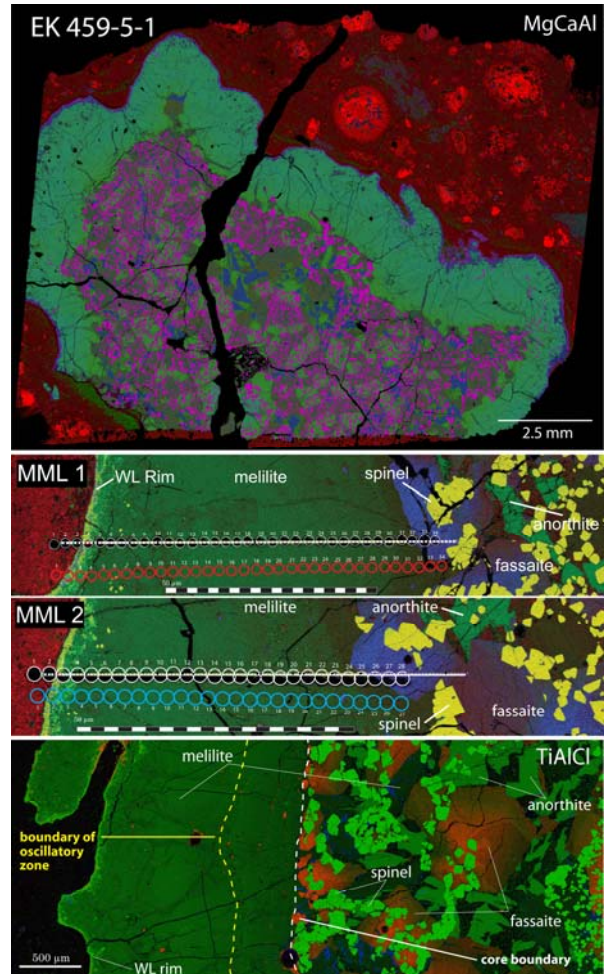


**Figure 1.** False colored qualitative 3 element x-ray maps. All labels are in RGB order (ex: MgCaAl; Mg-Red, Ca-Green, Al-Blue). (a) The entire studied grain, EK 459-5-1. (b) Both line scan transects across the melilite mantle, white line: EMPA transect, white open circles: trace element ablation pits, blue/red open circles: isotope spot locations. All open circles are 50  $\mu\text{m}$  in diameter. Line scan localities relative to the whole grain can be seen in [7]. (c) X-ray map showing transitions between massive mantle, oscillatory zone and core-mantle boundary. Notice color change in melilite (darker, more åkermanitic melilite) as well as truncation of chlorine (blue) and Ti zoning in fassaite (edge of core vs. interior).

rim-core position so there is a net positive, core-ward trend to both. The variation seen from rim to core is  $\sim\text{Åk}_{42}$  to  $\text{Åk}_{72}$  and  $\sim\text{Åk}_{46}$  to  $\text{Åk}_{71}$  for MML1 and MML2, respectively. There is a 1% increase in  $\delta^{25}\text{Mg}$  from rim to core for both line scans. Additionally, both

line scans exhibit a notable change in  $\delta^{25}\text{Mg}$  between the massive and the oscillatory zones of the mantle (Fig. 2, 3) but no measurable difference between the core and mantle melilite. Both line scans show a steady decrease in  $\delta^{25}\text{Mg}$  from the oscillatory zone to the massive zone. The massive section of the mantle shows variable major element patterns (seen as  $\text{\AA}k_{\#}$  in Fig. 2) as well as  $\delta^{25}\text{Mg}$ . Trace element variations also exist between oscillatory zoned and massive sections, although not consistent between line scans. The trace element abundances are discussed in [7].

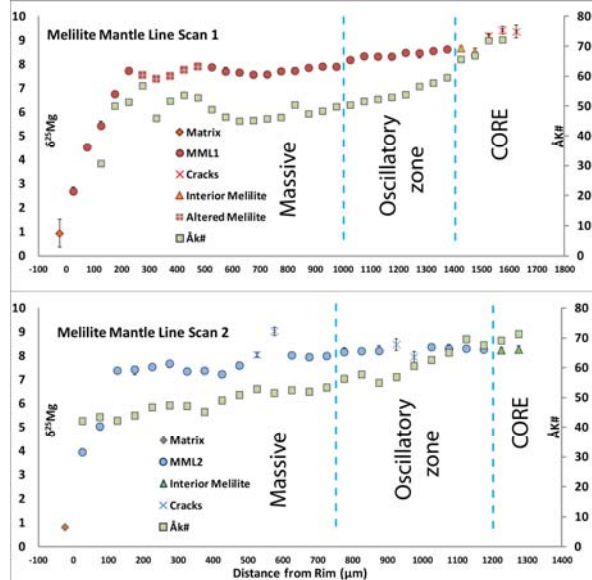


**Figure 2**  $\delta^{25}\text{Mg}$  and  $\text{\AA}k_{\#}$  plotted vs. distance from rim. This is the complete transverse for both line scans. Cracks and obvious sections of alteration are indicated. The transitions between core, oscillatory zone and massive section are indicated with a dashed blue line. All error is reported as  $2\sigma$ , much of the error is smaller than the data points.

**Discussion:** The sharp decrease in  $\delta^{25}\text{Mg}$  from  $\sim 7$ -8 to 1 ‰ towards the rim is likely a late stage event signified by a disturbance in  $^{26}\text{Al}$ - $^{26}\text{Mg}$  systematics (loss of  $^{26}\text{Mg}^*$ ) but this is not well constrained. Our data is consistent with previous hypotheses [8, 9] that this event seems to mark a period of open system isotopic exchange with an adjacent reservoir of chondritic value, at least with regards to  $\delta^{25}\text{Mg}$ .

Crosscutting relationships imply that the core of this CAI had to have been in place before the formation of the present mantle as evidenced by truncation of Cl rich zones in the core lithology (Fig. 1c). A normally zoned outward-in crystallization sequence due to localized surficial volatile depletion as presented in [10] does not seem to be the likely formation mechanism for EK 459-5-1. The core of EK 459-5-1 persisted through the melting event[s] which formed the mantle. The isotopic profile presented here does

not agree with a complete outside-in crystallization model, as initial surficial melilite crystallization would render the CAI a closed system yielding no mechanism for core-ward enrichment in  $\delta^{25}\text{Mg}$  [9].

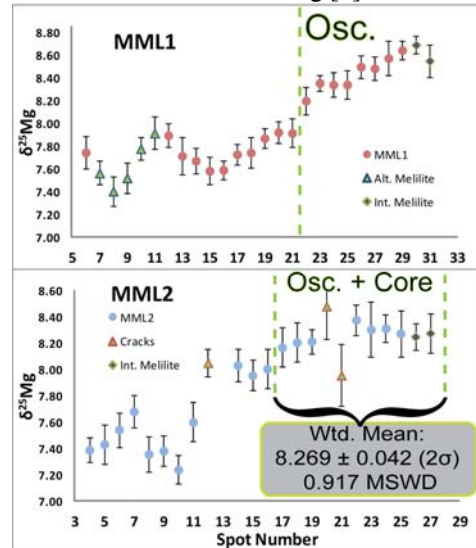


**Figure 3.** Line scans with rim-ward data removed (and the points lying on interior cracks in MML1) to further interpret trends and present the resolution of the data. The core melilite  $\delta^{25}\text{Mg}$  values are essentially the same as the first onset of the mantle. In MML2 the oscillatory zone and the core show a flat  $\delta^{25}\text{Mg}$  signature. The weighted mean of these sections was calculated ignoring the two data points which fell on cracks. MML1 on the other hand shows an almost constant decrease with a definite ‘step’ once the massive part of the mantle was reached.

$\delta^{25}\text{Mg}$  of the melilite in the core is essentially the same as the inner melilite mantle, indicating the same (or similar) source but from a different event as discussed above. The  $\delta^{25}\text{Mg}$  profile of MML2 (Fig. 3) appears to vary as a step function correlating to the separate petrologic zones of the mantle. This could be a record of multiple partial remelting events interacting with different reservoirs of  $\delta^{25}\text{Mg}$  or entirely different material altogether. This profile is not seen in MML1, although the variation (and subsequent decrease) between mantle zones is. It is clear that distinct petrologic, chemical and isotopic zones exist within this CAI, correlating to a diverse, multi-stage history.

**References:** [1] Bouvier A. and Wadhwa M. (2010) *Nature Geosci*, 3, 637-641. [2] Wark D. A. and Lovering J. F. (1982) *GCA*, 46, 2581-2594. [3] El Goresy A. et al. (1985) *GCA*, 47, 1635-1650. [4] Meeker G. P. (1995) *MAPS*, 30, 71-84. [5] Young E. D. and Galy A. (2004) *RIMG*, 55, 197-230. [6] Davis A. M. et al. (1990) *Nature*, 347, 655-658. [7] Jeffcoat C. R. et al. (2014) *LPS XLV Abstract #2523*. [8] Simon J. I. et al. (2005) *EPSL*, 238, 272-283. [9] Simon J. I. and Young E. D. (2011) *EPSL*, 304, 468-482. [10] Mendybaev R. A. (2006) *GCA*, 70, 2622-2642. [11] Richter F. M. et al. (2006) *MAPS*, 41, 83-93.